Tuning Quantum Dot Luminescence Below the Bulk Band Gap Using Tensile Strain

Paul J. Simmonds,[†,‡,∥,*] Christopher D. Yerino,[†,∥] Meng Sun,[§] Baolai Liang,[‡] Diana L. Huffaker,[‡,§] Vitaliy G. Dorogan,[⊥] Yuriy Mazur,[⊥] Gregory Salamo,[⊥] and Minjoo Larry Lee[†,*]

[†]Department of Electrical Engineering, Yale University, P.O. Box 208284, New Haven, Connecticut 06520, United States, [‡]California NanoSystems Institute and [§]Department of Electrical Engineering, University of California, Los Angeles, California 90095, United States, and [⊥]Institute for Nanoscience and Engineering, University of Arkansas, Fayetteville, Arkansas 72701, United States. [∥]These authors contributed equally to this work.

ABSTRACT Self-assembled quantum dots (SAQDs) grown under biaxial tension could enable novel devices by taking advantage of the strong band gap reduction induced by tensile strain. Tensile SAQDs with low optical transition energies could find application in the technologically important area of mid-infrared optoelectronics. In the case of Ge, biaxial tension can even cause a highly desirable crossover from an indirect- to a direct-gap band structure. However, the inability to grow tensile SAQDs without dislocations has impeded progress in these directions. In this article, we demonstrate a method to grow dislocation-free, tensile SAQDs by employing the unique strain relief mechanisms of (110)-oriented surfaces. As a model system, we show that tensile GaAs SAQDs form spontaneously, controllably, and without dislocations on InAlAs(110) surfaces. The tensile strain reduces the band gap in GaAs SAQDs by ~40%, leading to robust type-I quantum confinement and photoluminescence at energies lower than that of bulk GaAs. This method can be extended to other zinc blende and diamond cubic materials to form novel optoelectronic devices based on tensile SAQDs.

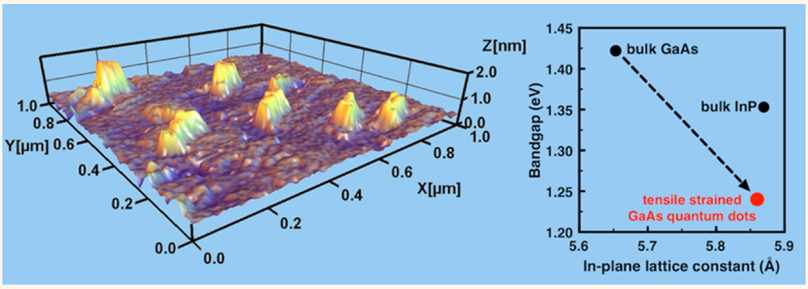

KEYWORDS: quantum dots · self-assembled growth · molecular beam epitaxy · tensile strain · band gap engineering · strain engineering · InP(110)

Self-assembled quantum dots (SAQDs) have found abundant uses owing to their tunable light emission and atom-like electronic properties.[1,2] To date, research has been restricted almost exclusively to SAQD systems under compressive strain, with tensile-strained SAQDs receiving little attention due to difficulties with their growth.[3,4] In typical SAQDs, quantum confinement effects and compressive strain work together to shift optical transitions to energies much higher than that of the bulk; for InAs SAQDs on GaAs, photoluminescence (PL) is typically observed at energies ~0.6−0.7 eV higher than the bulk band gap of InAs.[5] However, tensile strain substantially decreases band gap energies,[6,7] and SAQDs grown under tension could have *lower* transition energies than in the bulk. Tensile strain therefore represents a vast, untapped resource for tuning SAQD properties for novel optoelectronic devices. This work discusses a general method for growing tensile-strained SAQDs, using GaAs on $In_{0.48}Al_{0.52}As$/InP as a model system.

The ability to grow tensile-strained SAQDs from III−V and group IV semiconductors would be particularly valuable for mid-infrared optoelectronics. Mid-infrared (mid-IR) devices operating in the wavelength range of $\lambda \sim 2-10\ \mu$m hold technological importance for applications as diverse as trace gas detection, *in vivo* diagnostics, and environmental monitoring.[8,9] Under tension, a typical SAQD strain of 4% would lower the band gap of most III−V semiconductors by ~0.5 eV,[7] pushing materials with already low bulk band gap energies (*e.g.*, ~0.6−1.0 eV) well into the mid-IR range (~0.1−0.6 eV). A method for self-assembled growth under tensile strain

* Address correspondence to pjsimmonds@cnsi.ucla.edu, minjoo.lee@yale.edu.

Received for review January 24, 2013 and accepted May 23, 2013.

Published online May 23, 2013
10.1021/nn400395y

could also create new ways to enhance the properties of Ge by converting it from an indirect- to a direct-gap semiconductor.[10] While Ge is traditionally regarded as a nonluminescent material, a tensile strain of 2−4% would theoretically enable it to act as an efficient light emitter, with tunable luminescence far into the mid-IR.[10,11] Recent research on tensile Ge has resulted in Ge-on-Si detectors,[12] light-emitting diodes,[13] and lasers,[14] as well as Ge nanomembranes[15] and nanowires[16] stretched by microelectromechanical systems. In comparison with these methods, tensile SAQDs would be a much more robust way to exploit the unique band engineering possibilities afforded by tensile strain.

To date, however, a reliable method for the growth of tensile SAQDs has yet to be established. Unlike compressive SAQDs grown in the Stranski−Krastanov mode, the formation of dislocations tends to adversely affect SAQDs grown under tensile strain.[3,17] Few reports on the growth of tensile SAQDs with favorable properties exist,[18−22] and among conventional zinc blende semiconductors, only type-II GaAs/Ga(As)Sb SAQDs have shown optical activity under tension.[20,22]

Recently, we proposed a model for SAQD growth, predicting that defect-free self-assembly can occur for any zinc blende semiconductor under tensile strain given the proper choice of substrate orientation—in particular, growth on (110) and (111) surfaces.[23] We successfully applied this model to achieve the dislocation-free self-assembly of tensile GaP nanoislands on GaAs(110) and (111)A,[23−25] although GaP/GaAs is optically inactive. In this present work, we demonstrate the generality of our tensile SAQD model by growing tensile GaAs SAQDs on $In_{0.52}Al_{0.48}As$/InP(110). We confirm that dislocation-free self-assembly takes place using atomic force microscopy and transmission electron microscopy. The tensile GaAs SAQDs are optically active, and their temperature-dependent PL behavior indicates photonic and electronic properties analogous to those of conventional compressive SAQDs. Furthermore, we show for the first time optical transitions from type-I SAQDs with energy 0.2 eV *below* the bulk band gap, consistent with strong band gap reduction due to tensile strain.

RESULTS AND DISCUSSION

The model presented in ref 23 shows that the self-assembly of nanostructures competes with the formation of dislocations to relax strain during epitaxial growth. For conventional SAQDs, dislocation-free self-assembly occurs preferentially since dislocation nucleation is naturally suppressed in compressively strained materials grown on (001) surfaces.[23] For the case of tensile materials, (110) or (111) surfaces inhibit dislocation nucleation much more effectively than (001), creating the opportunity for SAQDs to form.[23] In this present work, we used molecular beam epitaxy

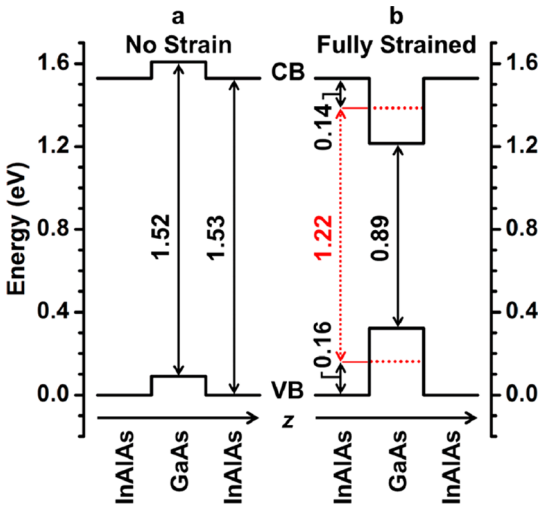

Figure 1. Band gap reduction in SAQDs due to tensile strain. Calculated conduction band (CB) and valence band (VB) alignment at 20 K is shown for $In_{0.52}Al_{0.48}As$(110) barriers surrounding GaAs SAQDs: (a) without strain, and (b) with GaAs fully strained to the InAlAs. In (b), the 3.7% lattice mismatch with the InAlAs lowers the band gap of the GaAs SAQDs and produces type-I quantum confinement (*i.e.*, in both CB and VB). SAQD bound states (dotted lines) are calculated based on the average dimensions of 6 ML GaAs SAQDs in Figure 2d, with average height 2.6 nm in the *z*-direction. The transition energies shown have units of eV.

(MBE) to grow GaAs on $In_{0.52}Al_{0.48}As$(110), which has a 3.7% tensile lattice mismatch.[7] This material system is ideally suited to demonstrate tensile SAQD growth because the large tensile strain is predicted to reduce the band gap of GaAs by ∼0.6 eV and produce confinement for both electrons and holes (*i.e.*, type-I band alignment, Figure 1.). The $In_{0.52}Al_{0.48}As$ barriers (hereafter referred to as InAlAs) are lattice-matched to InP(110), which serves as the growth substrate.

Prior to GaAs SAQD growth, we investigated growth conditions for InAlAs on InP(110). MBE growth of III−V semiconductor materials with a (110) orientation is highly challenging due to the propensity for surface roughening.[26] However, by using a combination of very low growth temperature and high V/III flux ratio,[27] we obtain flat, optically active InAlAs on InP(110). The smooth InAlAs(110) surfaces have a root-mean-square roughness of 3.0 Å measured over an area 100 μm^2 by atomic force microscopy (AFM) (Figure 2a). We deposited 0−7 monolayers (ML) of GaAs onto InAlAs surfaces to investigate self-assembly. Where samples were grown for optical characterization, the GaAs was capped with a final layer of InAlAs.

Tensile SAQDs form spontaneously during the growth of GaAs on InAlAs(110) surfaces, as predicted by our self-assembly model.[23] One monolayer of GaAs deposited onto InAlAs forms flat, 2D islands with monolayer-high steps (Figure 2b). As the deposition amount is increased to 3 ML, the GaAs self-assembles into 3D nanostructures across the surface. The transition from 2D growth (Figure 2b) to 3D growth (Figure 2c,d)

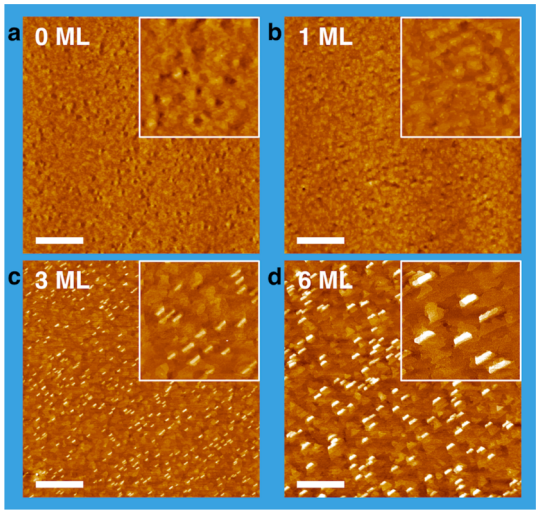

Figure 2. AFM images showing how the GaAs/InAlAs(110) surface morphology evolves with increasing GaAs deposition: (a) 0 ML, (b) 1 ML, (c) 3 ML, and (d) 6 ML. The scale bar in each represents 1 μm. The insets are higher magnification 1 μm^2 images. The out-of-plane scale in all images is 4 nm.

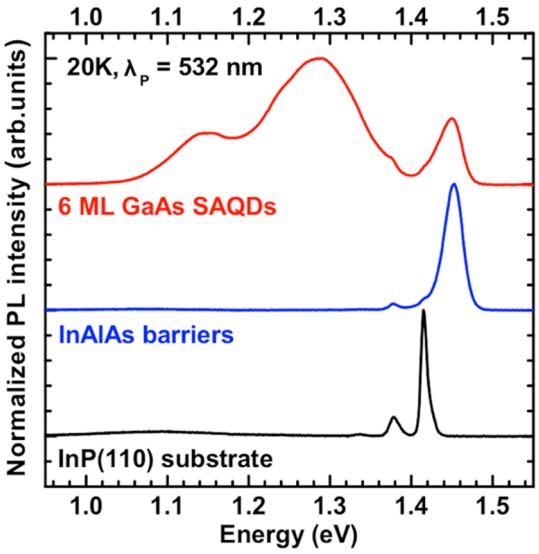

Figure 3. Comparison of PL spectra from (bottom) the bare InP(110) substrate, (middle) 300 nm InAlAs on InP(110) (*i.e.*, 0 ML GaAs SAQDs), (top) 6 ML GaAs SAQDs within 300 nm InAlAs on InP(110). Measurement temperature = 20 K, pump wavelength λ_P = 532 nm, pump excitation density = 13 W/cm^2.

during GaAs deposition is consistent with the Stranski–Krastanov mode in which nanostructure self-assembly is preceded by the formation of a planar wetting layer (WL). We note that this result offers a new method for the self-assembly of GaAs quantum dots, which typically are grown by droplet epitaxy on AlGaAs surfaces.[28]

We can control both the size and the areal density of these novel SAQDs, which is an important prerequisite for their future inclusion in optoelectronic devices. The 3 ML GaAs/InAlAs(110) nanostructures are approximately rectangular in shape with an average aspect ratio of 2.4 (Figure 2c). They are aligned parallel to [1$\bar{1}$0], with a length distribution of 80 $\pm$ 15 nm, a height distribution of 1.5 $\pm$ 0.2 nm, and an areal density of 1.9 $\times$ 10^9 cm^{-2}. Notably, the asymmetric morphology of our tensile GaAs/InAlAs SAQDs grown on InP(110) mirrors that of conventional compressively strained SAQDs based on InP(001) substrates.[29] Raising the GaAs deposition amount to 6 ML (Figure 2d) increases both the length and height of the SAQDs to 193 $\pm$ 26 and 2.6 $\pm$ 0.3 nm, respectively, while their aspect ratio remains almost constant at 2.2. At 6 ML, the increase in GaAs SAQD size is accompanied by a reduction in areal density to 7.3 $\times$ 10^8 cm^{-2}, likely due to ripening effects which are well-known in compressively strained SAQD systems.[30]

To investigate optical activity, we compared PL spectra from samples with and without tensile GaAs SAQDs at 20 K (Figure 3). Prior to sample growth, PL from the bare InP(110) substrate shows band edge recombination at 1.42 eV.[7] A small peak at ~1.38 eV is due to shallow donor–shallow acceptor pair recombination, and a weak defect band lies at ~1.1 eV due to Fe doping in the semi-insulating InP substrates.[31] A control sample consisting of a 300 nm InAlAs barrier layer grown on InP(110) reveals, in addition to the InP peaks, a PL signal from the InAlAs centered at 1.45 eV, with a full width at half-maximum (fwhm) of 27 meV (Figure 3). This PL emission energy is slightly lower than expected for InAlAs (1.53 eV at 20 K)[7] but is consistent with the work of Brown *et al.*, who attributed a similar reduction in energy to a defect-assisted transition.[27] The presence of defects within the InAlAs is perhaps unsurprising given that the low substrate temperature (300 °C) required for smooth growth will promote the incorporation of excess As and other point defects.[32] Despite this, PL emission is still seen at 300 K (see Figure S1 in Supporting Information), indicating that the InAlAs is of sufficient optical quality to act as a barrier material within which to embed GaAs SAQDs.

The tensile GaAs/InAlAs(110) SAQDs are optically active. We grew a repeat of the above InAlAs/InP(110) control sample but containing 6 ML GaAs, 100 nm below the surface. In Figure 3, the PL spectrum from this 6 ML GaAs sample exhibits a new peak with emission centered at 1.28 eV and a weaker shoulder peak close to 1.14 eV. Though its emission energy is well below that of bulk GaAs, we will show that the source of the main PL peak is recombination within the tensile GaAs SAQDs.

The emission energy of the main PL peak shows a dependence on tensile GaAs SAQD size that is expected due to quantum size effects.[33] Changing the GaAs deposition thickness enables us to control the size of the tensile-strained SAQDs (Figure 2c,d). Starting with 5 ML GaAs SAQDs, we are able to tune the peak PL emission to lower energy by increasing the size of the SAQDs to 6 ML and then 7 ML (Figure 4a).

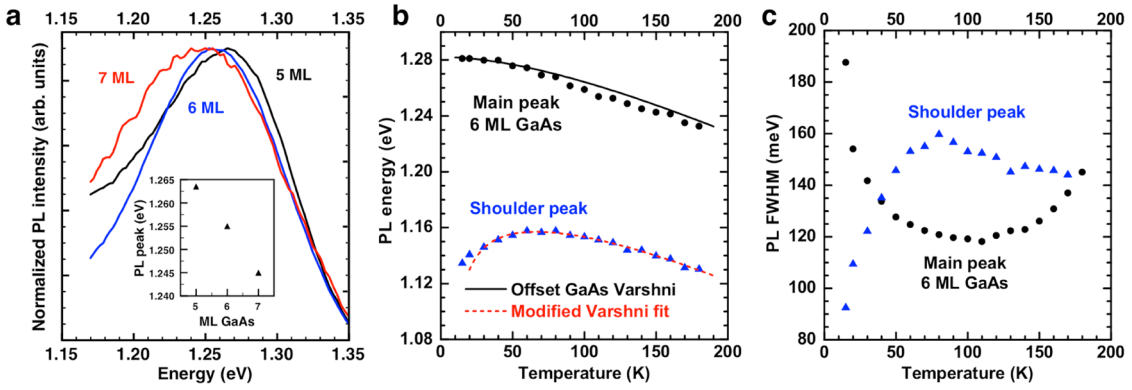

Figure 4. (a) Normalized PL spectra at 77 K from the main emission peak in 5, 6, and 7 ML GaAs SAQDs. The inset shows that the PL peak moves to lower energies as the amount of GaAs deposition is increased. (b) Variation in the main and shoulder peak energies from 6 ML GaAs SAQDs as a function of measurement temperature. PL data for the main peak are in good agreement with the general trend of the Varshni temperature dependence model for GaAs. For comparison to the data, the 0 K intercept of the bulk GaAs Varshni curve has been offset to 1.28 eV from its unstrained value (1.52 eV). The shoulder peak energy data fit a modified Varshni expression of the form in ref 37, suggesting carrier localization. (c) Temperature dependences of the main and shoulder PL peak linewidths from 6 ML GaAs SAQDs. The "u-shaped" response of the main peak is a characteristic of SAQD arrays. Pump excitation density = 13 W/cm^2.

As our SAQDs get larger, the energy separation between the SAQD ground state and the GaAs band edge gets smaller, and the PL emission energy is reduced accordingly.[33] The trend summarized by the inset to Figure 4a indicates that the observed PL emission is indeed from recombination between quantized states within the GaAs SAQDs.

Temperature-dependent PL measurements of the 6 ML GaAs sample confirm that the main PL peak in Figure 3 comes from an array of optically active SAQDs, while also revealing a pronounced reduction in band gap induced by the tensile strain (Figure 4b,c). As the measurement temperature T is increased from 15 K, the PL energy of the 6 ML main peak decreases (Figure 4b), in good agreement with the expected Varshni-type temperature dependence of the GaAs band gap.[7] In Figure 4b, the primary emission peak from the tensile 6 ML GaAs SAQDs is offset to a much lower energy than that of bulk, unstrained GaAs (1.28 eV as opposed to 1.52 eV at 20 K).[7] This energy reduction is consistent with the expected contraction of the GaAs band gap due to the tensile strain. For comparison, unstrained GaAs QDs grown by droplet epitaxy typically exhibit peak PL emission at 1.60–1.75 eV at 20 K,[28] which is higher than the bulk band gap energy of GaAs because of quantum confinement.

To understand the effect of tensile strain on the GaAs SAQD transition energies, we calculated the strained band alignment and quantum-confined energy states for 6 ML GaAs SAQDs at 20 K (Figure 1; see Methods section). Assuming that the 6 ML SAQDs are fully strained to the InAlAs, we expect the GaAs SAQD band gap to decrease from 1.52 to 0.89 eV. Our band alignment results shown in Figure 1b anticipate a type-I band structure. Based on the average dimensions of the 6 ML SAQDs, quantum confinement energies of 140 and 160 meV for electrons and holes, respectively, were calculated at 20 K. Our band gap model therefore predicts a transition energy of 1.22 eV between the electron and hole ground states, close to the 1.28 eV main PL peak energy measured at 20 K in Figure 4b. Refinement of our model in terms of SAQD shape, composition, and strain distribution will allow us to reduce the discrepancy. Nevertheless, these calculations indicate that the reduced PL energy of the SAQDs is largely accounted for by the reduction in GaAs band gap due to tensile strain. In addition, this model predicts robust type-I carrier confinement up to room temperature, which we have confirmed by the observation of PL from the SAQDs at 300 K (see Figures S1 and S2 in Supporting Information).

The temperature dependence of the main PL peak's fwhm in Figure 3 provides additional evidence that it arises due to emission from the tensile 6 ML GaAs SAQDs (Figure 4c). The peak width is the result of photon emission from many GaAs SAQDs with slightly different sizes and hence varying quantum confinement energies. Figure 4c shows that as T is increased from 15 K, the fwhm of the main peak is initially reduced, reaching a minimum of 118 meV at 110 K. A similar reduction in fwhm has been reported for compressive type-I InAs/GaAs(001) SAQDs and corresponds to quenching of PL from small dots as carriers escape into larger dots where the confined quantum states are lower in energy.[34−36] Above 110 K, we see the fwhm of the main peak increase due to carrier–phonon scattering and thermal broadening of the carrier distribution. This distinctive ensemble effect is characteristic of type-I quantum dot arrays and supports our conclusion that we have created optically active, tensile GaAs/InAlAs(110) SAQDs.

The source of the lower energy shoulder peak in Figure 3 is more ambiguous; the relative intensities of the main and shoulder peaks are independent of pump laser power density, ruling out an excited state as the cause of the double feature. However, the two peaks

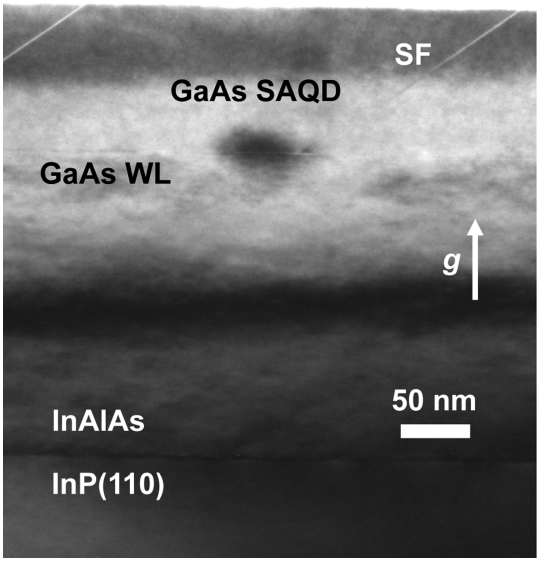

Figure 5. X-TEM image showing a single 6 ML GaAs SAQD surrounded by InAlAs. The thin horizontal line of the 2D GaAs wetting layer (WL) is visible. Stacking faults (SF) emerge from the lower InAlAs barrier and extend to the surface. The darker bands above and below the SAQD are imaging artifacts.

exhibit very different temperature-dependent PL behavior. Unlike the main peak, the shoulder peak transition energy diverges from the expected Varshni-type behavior below ~70 K (Figure 4b). A similar divergence, due to exciton localization in band-tail states, has been observed in a range of material systems such as GaAsBi[37] and GaInNAs quantum wells,[38] as well as conventional InAs SAQDs.[39] The temperature dependence of carrier localization is known to follow a modified Varshni relation,[40] which is indeed observed for the PL data of the shoulder peak (Figure 4b). As T is increased from 15 to 70 K, the transition energy of the shoulder peak increases as excitons become thermalizd out of their localized states. Then, at higher temperatures, we see the expected reduction in PL energy due to the standard Varshni-type temperature dependence of the GaAs band gap.[7] In Figure 4c, the "hump" in the shoulder peak fwhm as a function of temperature is also consistent with the presence of localization.[37] Given our earlier PL results from the InAlAs barriers and their relation to defect states, a likely cause of the observed localization is shallow traps that exist in bulk InAlAs with both (110)[27] and (001)[41] orientations.

The GaAs/InAlAs(110) SAQDs are dislocation-free, consistent with the predictions of our model for tensile self-assembly.[23] Cross-sectional transmission electron microscopy (X-TEM) shows strain contrast lobes surrounding a single buried 6 ML GaAs/InAlAs(110) dot (Figure 5). Contrast lobes such as these are characteristic of coherently strained, dislocation-free SAQDs.[42] The presence of a GaAs WL beneath the SAQD confirms the Stranski–Krastanov growth mode deduced from the AFM images in Figure 2. Outside of the GaAs layer, the microstructural quality of the InAlAs barriers is limited primarily by stacking faults (SFs). X-TEM of InAlAs samples with and without GaAs layers (not shown) revealed similar densities of stacking faults, indicating that SFs initiate in the lower InAlAs barrier and propagate upward during growth. Optimized InAlAs(110) growth conditions will help eliminate SFs and reduce the density of the trap states discussed above, resulting in GaAs SAQDs with improved optical quality. However, despite the limitations of the InAlAs barriers, the GaAs SAQDs themselves do not appear to nucleate new defects such as dislocations and thus have sufficient structural quality for luminescence up to room temperature (see Supporting Information).

CONCLUSION

By employing our new model for tensile-strained self-assembly,[23] we have created optically active, tensile GaAs quantum dots on InAlAs(110). Due to the strong band gap reduction induced by the tensile strain, this is the first reported PL emission from type-I quantum dots with peak energy *lower* than the bulk band gap. In agreement with our model for tensile self-assembly on (110) surfaces,[23] the SAQDs are coherently strained and do not nucleate dislocations. The size and density of the tensile SAQDs are readily controllable by adjusting the GaAs deposition thickness. The dependence of PL photon energy on both dot size and temperature confirms that the emission we observe originates from the tensile GaAs SAQDs, and that its overall behavior is similar to PL from traditional, compressively strained, type-I InAs/GaAs(001) SAQDs.

Taken in conjunction with our previous results in GaP/GaAs(110) and GaP/GaAs(111),[23–25] these dislocation-free GaAs/InAlAs(110) SAQDs confirm that tensile-strained self-assembly is not limited to a single material system. Instead, we expect dislocation-free, tensile self-assembly to be possible on the (110) and (111) surfaces of all zinc blende and related materials, including III–V and group IV semiconductors. Since GaAs and Ge have nearly the same lattice constant, the InAlAs buffers used here could also provide an important template for growth of Ge SAQDs under ~3.7% tensile strain. Our straightforward approach for accessing the almost entirely unexplored domain of tensile quantum dots could enable new SAQD technologies such as mid-IR lasers based on Ge or III–V materials.

METHODS

Sample Growth. The crystal growth of the GaAs/$In_{0.52}Al_{0.48}As$/InP(110) samples studied in this work was carried out by solid-source MBE. We used Fe-doped, semi-insulating, nominally on-axis (±0.5°) InP(110) substrates. These were mounted on 4 in. silicon handle wafers using high-purity molten indium

as an adhesive. The substrates underwent initial thermal degassing under ultrahigh vacuum conditions at 200 °C for 8 h and then 300 °C for 2 h, prior to loading into the MBE growth chamber.

MBE growth was performed using high-purity Al, Ga, and In effusion cells. As_4 was supplied from a valved source, with the cracker zone held at 600 °C to prevent pyrolysis to the As_2 dimer. Beam equivalent pressures (BEPs) for each species were determined using a beam flux monitor at the substrate location, while substrate temperature was measured with an optical pyrometer. All growth rates were calculated from reflection high-energy electron diffraction (RHEED) intensity oscillations.

The InP(110) substrates were thermally degassed in the growth chamber at 500 °C for 30 min, under an As_4 BEP of approximately 3.5×10^{-5} Torr. We grew 200 nm lattice-matched InAlAs at 300 °C, with a V/III BEP ratio of 80 and a growth rate of 0.5 μm/h, before annealing under As_4 at 500 °C for 15 min to promote surface smoothing. We deposited 0−7 ML GaAs onto the InAlAs at 500 °C, with a V/III BEP ratio of 65 and a growth rate of 0.1 ML/s. Samples were then either immediately cooled to 200 °C under an As_4 flux, or the GaAs was capped with 100 nm of InAlAs (grown under identical conditions to the lower InAlAs barrier) before cooling.

Due to the low areal densities ($<2 \times 10^9$ cm^{-2}) and heights (<3 nm) of our tensile GaAs SAQDs, RHEED is unsuitable for observing the 2D−3D growth transition of the Stranski−Krastanov mode during self-assembly.[43] Even after dot nucleation has occurred, the vast majority of the electron beam continues to diffract from the 2D wetting layer surface rather than the 3D SAQDs, so the RHEED pattern remains streaky throughout. Instead, we used the amount of GaAs in the SAQDs to estimate the 2D−3D transition thickness.[44] From AFM data, we calculated the total volume of the SAQDs per unit area for the 3 and 6 ML samples. Extrapolating from these two data points suggests that the 2D−3D transition occurs after ~1.6 ML GaAs has been deposited.

Sample Characterization. After removing the samples from the MBE chamber, we used AFM in tapping mode to study surface morphology. We calibrated InAlAs composition using symmetric (440) X-ray diffraction rocking curves. By compiling reciprocal space maps, we confirmed that the lattice-matched InAlAs barriers were minimally strained with respect to the InP(110). For X-TEM, we mechanically thinned the InP-based samples and then used low-angle Ar ion milling to reduce their thickness to electron transparency. We imaged the prepared samples along the in-plane [1$\bar{1}$0] zone axis with a transmission electron microscope operated at 200 kV. X-TEM was performed with a $g = \langle 220 \rangle$ two-beam diffraction condition to accentuate the strain contrast of the SAQDs as well as any extended defects within the sample.

We investigated the optical characteristics of the buried GaAs SAQDs with temperature-dependent PL measurements. Samples were mounted inside a closed-cycle He optical cryostat with temperature control over the range of 10−300 K. A frequency-doubled neodymium-doped yttrium aluminum garnet laser was used as the pump laser with wavelength λ_P = 532 nm. The laser beam was focused on sample surfaces using a short-focus objective lens with 50× magnification to a spot with diameter of ~20 μm. Since the sample was <1 cm from the cryostat window, we could use the same objective lens to also collect the PL signal. The PL signal was dispersed with a 0.5 m imaging triple grating monochromator and detected by a liquid-nitrogen-cooled InGaAs linear photodiode array. We varied the excitation density over the range of 10^{-2} to 10^4 mW using a set of neutral density filters. For each spectral PL feature observed, we found values for peak energy, fwhm, and integrated intensity using multiple Gaussian fits.

Band Alignment Calculation. Electronic band alignments were calculated for the GaAs SAQDs surrounded by $In_{0.52}Al_{0.48}As$(110) using the approach of Van de Walle,[45] with valence band offsets taken from Tiwari and Frank.[46] Band gaps, elastic constants, deformation potentials, and effective masses were given by Vurgaftman *et al.*[7] To incorporate the effect of strain on band alignments, the SAQDs were assumed to be fully pseudomorphic to the InAlAs. Expressions specific to the (110) crystal orientation were used to account for biaxial strain in the SAQDs and the resultant splitting of the light hole and heavy hole bands.[45] Quantized bound states within the SAQDs were calculated using a "particle in a finite box" model. To simplify the calculation, the SAQD shape was assumed to be a rectangular prism with dimensions given by the AFM measurements.

Conflict of Interest: The authors declare no competing financial interest.

Acknowledgment. Microscopy facilities used in this work were supported by the Yale Institute for Nanoscience and Quantum Engineering and National Science Foundation MRSEC DMR 1119826. C.D.Y. acknowledges support from the Department of Energy Office of Science Graduate Fellowship Program (DOE SCGF), made possible in part by the American Recovery and Reinvestment Act of 2009, administered by ORISE-ORAU under Contract No. DE-AC05-06OR23100.

Supporting Information Available: Room temperature PL spectra and temperature-dependent PL data showing emission from tensile GaAs SAQDs over the range of 15−300 K. This material is available free of charge *via* the Internet at http://pubs.acs.org.

REFERENCES AND NOTES

1. Leonard, D.; Krishnamurthy, M.; Reaves, C. M.; Denbaars, S. P.; Petroff, P. M. Direct Formation of Quantum-Sized Dots from Uniform Coherent Islands of InGaAs on GaAs Surfaces. *Appl. Phys. Lett.* **1993**, *63*, 3203–3205.
2. Eaglesham, D. J.; Cerullo, M. Dislocation-Free Stranski−Krastanow Growth of Ge on Si(100). *Phys. Rev. Lett.* **1990**, *64*, 1943–1946.
3. Pachinger, D.; Groiss, H.; Lichtenberger, H.; Stangl, J.; Hesser, G.; Schäffler, F. Stranski−Krastanow Growth of Tensile Strained Si Islands on Ge (001). *Appl. Phys. Lett.* **2007**, *91*, 233106.
4. Taliercio, T.; Gassenq, A.; Luna, E.; Trampert, A.; Tournié, E. Highly Tensile-Strained, Type-II, $Ga_{1-x}In_xAs$/GaSb Quantum Wells. *Appl. Phys. Lett.* **2010**, *96*, 062109.
5. Ustinov, V. M.; Maleev, N. A.; Zhukov, A. E.; Kovsh, A. R.; Egorov, A. Y.; Lunev, A. V.; Volovik, B. V.; Krestnikov, I. L.; Musikhin, Y. G.; Bert, N. A.; *et al.* InAs/InGaAs Quantum Dot Structures on GaAs Substrates Emitting at 1.3 μm. *Appl. Phys. Lett.* **1999**, *74*, 2815–2817.
6. Kuo, C. P.; Vong, S. K.; Cohen, R. M.; Stringfellow, G. B. Effect of Mismatch Strain on Band Gap in III−V Semiconductors. *J. Appl. Phys.* **1985**, *57*, 5428–5432.
7. Vurgaftman, I.; Meyer, J. R.; Ram-Mohan, L. R. Band Parameters for III−V Compound Semiconductors and Their Alloys. *J. Appl. Phys.* **2001**, *89*, 5815–5875.
8. Bakhirkin, Y. A.; Kosterev, A. A.; Roller, C.; Curl, R. F.; Tittel, F. K. Mid-Infrared Quantum Cascade Laser Based Off-Axis Integrated Cavity Output Spectroscopy for Biogenic Nitric Oxide Detection. *Appl. Opt.* **2004**, *43*, 2257–2266.
9. Guo, B.; Wang, Y.; Peng, C.; Zhang, H.; Luo, G.; Le, H.; Gmachl, C.; Sivco, D.; Peabody, M.; Cho, A. Laser-Based Mid-Infrared Reflectance Imaging of Biological Tissues. *Opt. Express* **2004**, *12*, 208–219.
10. Kurdi, M.; El Fishman, G.; Sauvage, S.; Boucaud, P. Band Structure and Optical Gain of Tensile-Strained Germanium Based on a 30 Band k·p Formalism. *J. Appl. Phys.* **2010**, *107*, 013710.
11. Dutt, B.; Sukhdeo, D. S.; Nam, D.; Vulovic, B. M.; Yuan, Z.; Saraswat, K. C. Roadmap to an Efficient Germanium-on-Silicon Laser: Strain *vs.* n-Type Doping. *IEEE Photonics J.* **2012**, *4*, 2002–2009.
12. Liu, J.; Cannon, D. D.; Wada, K.; Ishikawa, Y.; Jongthammanurak, S.; Danielson, D. T.; Michel, J.; Kimerling, L. C. Tensile Strained Ge p-i-n Photodetectors on Si Platform for C and L Band Telecommunications. *Appl. Phys. Lett.* **2005**, *87*, 011110.
13. Sun, X.; Liu, J.; Kimerling, L. C.; Michel, J. Room-Temperature Direct Bandgap Electroluminesence from Ge-on-Si Light-Emitting Diodes. *Opt. Lett.* **2009**, *34*, 1198–1200.

14. Liu, J.; Sun, X.; Camacho-Aguilera, R.; Kimerling, L. C.; Michel, J. Ge-on-Si Laser Operating at Room Temperature. *Opt. Lett.* **2010**, *35*, 679–681.
15. Sánchez-Pérez, J. R.; Boztug, C.; Chen, F.; Sudradjat, F. F.; Paskiewicz, D. M.; Jacobson, R. B.; Lagally, M. G.; Paiella, R. Direct-Bandgap Light-Emitting Germanium in Tensilely Strained Nanomembranes. *Proc. Natl. Acad. Sci. U.S.A.* **2011**, *108*, 18893–18898.
16. Greil, J.; Lugstein, A.; Zeiner, C.; Strasser, G.; Bertagnolli, E. Tuning the Electro-optical Properties of Germanium Nanowires by Tensile Strain. *Nano Lett.* **2012**, *12*, 6230–6234.
17. Pachinger, D.; Groiss, H.; Teuchtmann, M.; Hesser, G.; Schäffler, F. Surfactant-Mediated Si Quantum Dot Formation on Ge(001). *Appl. Phys. Lett.* **2011**, *98*, 223104.
18. Pinczolits, M.; Springholz, G.; Bauer, G. Direct Formation of Self-Assembled Quantum Dots under Tensile Strain by Heteroepitaxy of PbSe on PbTe(111). *Appl. Phys. Lett.* **1998**, *73*, 250–252.
19. Raviswaran, A.; Liu, C.-P.; Kim, J.; Cahill, D. G.; Gibson, J. M. Evolution of Coherent Islands during Strained-Layer Volmer–Weber Growth of Si on Ge(111). *Phys. Rev. B* **2001**, *63*, 125314.
20. Toropov, A. A.; Lyublinskaya, O. G.; Meltser, B. Y.; Solov'ev, V. A.; Sitnikova, A. A.; Nestoklon, M. O.; Rykhova, O. V.; Ivanov, S. V.; Thonke, K.; Sauer, R. Tensile-Strained GaAs Quantum Wells and Quantum Dots in a $GaAs_xSb_{1-x}$ Matrix. *Phys. Rev. B* **2004**, *70*, 205314.
21. Pohjola, P.; Hakkarainen, T.; Koskenvaara, H.; Sopanen, M.; Lipsanen, H.; Sainio, J. Tensile-Strained GaAsN Quantum Dots on InP. *Appl. Phys. Lett.* **2007**, *90*, 172110.
22. Lin, T. C.; Wu, Y. H.; Li, L. C.; Sung, Y. T.; Lin, S. D.; Chang, L.; Suen, Y. W.; Lee, C. P. Electron Delocalization of Tensily Strained GaAs Quantum Dots in GaSb Matrix. *J. Appl. Phys.* **2010**, *108*, 123503.
23. Simmonds, P. J.; Lee, M. L. Tensile-Strained Growth on Low-Index GaAs. *J. Appl. Phys.* **2012**, *112*, 054313.
24. Simmonds, P. J.; Lee, M. L. Tensile Strained Island Growth at Step-Edges on GaAs(110). *Appl. Phys. Lett.* **2010**, *97*, 153101.
25. Simmonds, P. J.; Lee, M. L. Self-Assembly on (111)-Oriented III–V Surfaces. *Appl. Phys. Lett.* **2011**, *99*, 123111.
26. Yoshita, M.; Akiyama, H.; Pfeiffer, L. N.; West, K. W. Surface-Morphology Evolution during Growth-Interrupt *In Situ* Annealing on GaAs(110) Epitaxial Layers. *J. Appl. Phys.* **2007**, *101*, 103541.
27. Brown, A. S.; Metzger, R. A.; Henige, J. A. Growth and Properties of AlInAs–GaInAs Alloys and Quantum Wells on (110) InP. *J. Vac. Sci. Technol., B* **1993**, *11*, 817–819.
28. Watanabe, K.; Koguchi, N.; Gotoh, Y. Fabrication of GaAs Quantum Dots by Modified Droplet Epitaxy. *Jpn. J. Appl. Phys.* **2000**, *39*, L79–81.
29. Bierwagen, O.; Masselink, W. T. Self-Organized Growth of InAs Quantum Wires and Dots on InP(001): The Role of Vicinal Substrates. *Appl. Phys. Lett.* **2005**, *86*, 113110.
30. Krzyzewski, T. J.; Jones, T. S. Ripening and Annealing Effects in InAs/GaAs(001) Quantum Dot Formation. *J. Appl. Phys.* **2004**, *96*, 668–674.
31. Eaves, L.; Smith, A. W.; Skolnick, M. S.; Cockayne, B. An Investigation of the Deep Level Photoluminescence Spectra of InP(Mn), InP(Fe), and of Undoped InP. *J. Appl. Phys.* **1982**, *53*, 4955–4963.
32. Metzger, R. A.; McCray, L. G. X-ray and Photoluminescence Characterization of Low-Temperature AlInAs Grown by Molecular Beam Epitaxy. *Appl. Phys. Lett.* **1992**, *61*, 2196–2198.
33. Yamauchi, T.; Matsuba, Y.; Bolotov, L.; Tabuchi, M.; Nakamura, A. Correlation between the Gap Energy and Size of Single InAs Quantum Dots on GaAs(001) Studied by Scanning Tunneling Spectroscopy. *Appl. Phys. Lett.* **2000**, *77*, 4368–4370.
34. Xu, Z.; Lu, Z.; Yang, X.; Yuan, Z.; Zheng, B.; Xu, J.; Ge, W.; Wang, Y.; Wang, J.; Chang, L. Carrier Relaxation and Thermal Activation of Localized Excitons in Self-Organized InAs Multilayers Grown on GaAs Substrates. *Phys. Rev. B* **1996**, *54*, 11528–11531.
35. Lubyshev, D. I.; González-Borrero, P. P.; Marega, E.; Petitprez, E.; Scala, N. La; Basmaji, P. Exciton Localization and Temperature Stability in Self-Organized InAs Quantum Dots. *Appl. Phys. Lett.* **1996**, *68*, 205–207.
36. Heitz, R.; Mukhametzhanov, I.; Madhukar, A.; Hoffmann, A.; Bimberg, D. Temperature Dependent Optical Properties of Self-Organized InAs/GaAs Quantum Dots. *J. Electron. Mater.* **1999**, *28*, 520–527.
37. Mohmad, A. R.; Bastiman, F.; Ng, J. S.; Sweeney, S. J.; David, J. P. R. Photoluminescence Investigation of High Quality $GaAs_{1-x}Bi_x$ on GaAs. *Appl. Phys. Lett.* **2011**, *98*, 122107.
38. Bank, S. R.; Wistey, M. A.; Yuen, H. B.; Lordi, V.; Gambin, V. F.; Harris, J. S. Effects of Antimony and Ion Damage on Carrier Localization in Molecular-Beam-Epitaxy-Grown GaInNAs. *J. Vac. Sci. Technol., B* **2005**, *23*, 1320–1323.
39. Dai, Y. T.; Fan, J. C.; Chen, Y. F.; Lin, R. M.; Lee, S. C.; Lin, H. H. Temperature Dependence of Photoluminescence Spectra in InAs/GaAs Quantum Dot Superlattices with Large Thicknesses. *J. Appl. Phys.* **1997**, *82*, 4489–4492.
40. Eliseev, P. G.; Perlin, P.; Lee, J.; Osiński, M. "Blue" Temperature-Induced Shift and Band-Tail Emission in InGaN-Based Light Sources. *Appl. Phys. Lett.* **1997**, *71*, 569–571.
41. Capotondi, F.; Biasiol, G.; Vobornik, I.; Sorba, L.; Giazotto, F.; Cavallini, A.; Fraboni, B. Two-Dimensional Electron Gas Formation in Undoped $In_{0.75}Ga_{0.25}As/In_{0.75}Al_{0.25}As$ Quantum Wells. *J. Vac. Sci. Technol., B* **2004**, *22*, 702–706.
42. Leonard, D.; Krishnamurthy, M.; Fafard, S.; Merz, J. L.; Petroff, P. M. Molecular-Beam Epitaxy Growth of Quantum Dots from Strained Coherent Uniform Islands of InGaAs on GaAs. *J. Vac. Sci. Technol., B* **1994**, *12*, 1063–1066.
43. Alloing, B.; Zinoni, C.; Li, L. H.; Fiore, A.; Patriarche, G. Structural and Optical Properties of Low-Density and In-Rich InAs/GaAs Quantum Dots. *J. Appl. Phys.* **2007**, *101*, 024918.
44. Krzyzewski, T. J.; Joyce, P. B.; Bell, G. R.; Jones, T. S. Scaling Behavior in InAs/GaAs(001) Quantum-Dot Formation. *Phys. Rev. B* **2002**, *66*, 201302(R).
45. Van de Walle, C. G. Band Lineups and Deformation Potentials in the Model-Solid Theory. *Phys. Rev. B* **1989**, *39*, 1871.
46. Tiwari, S.; Frank, D. J. Empirical Fit to Band Discontinuities and Barrier Heights in III–V Alloy Systems. *Appl. Phys. Lett.* **1992**, *60*, 630–632.